NANO LETTERS

Letter

pubs.acs.org/NanoLett

Rational Design of Sub-Parts per Million Specific Gas Sensors Array Based on Metal Nanoparticles Decorated Nanowire Enhancement-Mode Transistors

Xuming Zou,[†] Jingli Wang,[†] Xingqiang Liu,[†] Chunlan Wang,[†] Ying Jiang,[‡] Yong Wang,[‡] Xiangheng Xiao,[†] Johnny C. Ho,*[,§] Jinchai Li,[†] Changzhong Jiang,[†] Ying Fang,[∥] Wei Liu,[†] and Lei Liao*[,†]

[†]Department of Physics and Key Laboratory of Artificial Micro- and Nano-structures of Ministry of Education, Wuhan University, Wuhan 430072, China

[‡]Department of Materials Sciences & Engineering, Zhejiang University, Zhejiang 310058, China

[§]Department of Physics and Materials Science, City University of Hong Kong, Tat Chee Avenue, Kowloon, Hong Kong SAR, China

[∥]National Center for Nanoscience and Technology, Beijing, 100190, China

Supporting Information

ABSTRACT: "One key to one lock" hybrid sensor configuration is rationally designed and demonstrated as a direct effective route for the target-gas-specific, highly sensitive, and promptly responsive chemical gas sensing for room temperature operation in a complex ambient background. The design concept is based on three criteria: (i) quasi-one-dimensional metal oxide nanostructures as the sensing platform which exhibits good electron mobility and chemical and thermal stability; (ii) deep enhancement-mode field-effect transistors (E-mode FETs) with appropriate threshold voltages to suppress the nonspecific sensitivity to all gases (decouple the selectivity and sensitivity away from nanowires); (iii) metal nanoparticle decoration onto the nanostructure surface to introduce the gas specific selectivity and sensitivity to the sensing platform. In this work, using Mg-doped In_2O_3 nanowire E-mode FET sensor arrays decorated with various discrete metal nanoparticles (i.e., Au, Ag, and Pt) as illustrative prototypes here further confirms the feasibility of this design. Particularly, the Au decorated sensor arrays exhibit more than 3 orders of magnitude response to the exposure of 100 ppm CO among a mixture of gases at room temperature. The corresponding response time and detection limit are as low as ~4 s and ~500 ppb, respectively. All of these could have important implications for this "one key to one lock" hybrid sensor configuration which potentially open up a rational avenue to the design of advanced-generation chemical sensors with unprecedented selectivity and sensitivity.

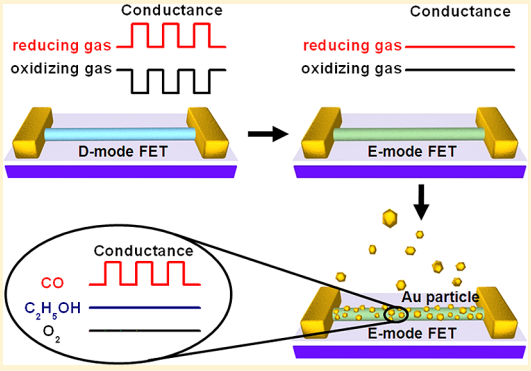

KEYWORDS: *In_2O_3 nanowires, transistors, enhancement-mode, gas sensors, selectivity*

In the past few decades, chemical gas sensing is perceived as one of the most important technological developments for the chemical process control, personal safety, and environmental sustainability, and so forth.[1−6] High selectivity and sensitivity, fast response, room-temperature operation, and long-term reliability are the key requirements for practical operations of these sensors.[7−13] In this regard, among various active sensing materials, quasi-one-dimensional metal oxide nanostructures, such as nanowires and nanobelts, have been extensively investigated due to their extraordinary surface-to-volume ratio and excellent chemical and thermal stabilities under a wide spectrum of operating conditions.[14−17] For example, Comini et al. explored single-crystalline SnO_2 nanobelts for the effective detection of CO, NO_2, and C_2H_5OH down to the ppm level by modulating the operating temperature between 300 and 400 °C.[18] Pd-doped SnO_2 nanofibers were also exploited for the selective detection of C_2H_5OH.[19] Later, besides employing a single sensing element, Sysoev and co-workers developed a hybrid sensor arrays composed of individual pristine SnO_2, surface doped (Ni)-SnO_2 nanowires, and TiO_2 and In_2O_3 whiskers, capable of differentiating between H_2 and CO reducing gases in the O_2 background.[20] However, all of these reported studies have relied on the gas sensing mechanism by reading signal outputs from the sensing elements in which the signals are mostly overlapping but with different gas selectivity and sensitivity. Instead of identifying the specific target gas with a dedicated sensor element, these mixed signals, potentially redundant and fault tolerant, would make the gas discrimination implicit and require tedious data processing/analysis via various pattern recognition schemes.[20−24] Until now, it is still an unresolved

Received: April 25, 2013
Revised: June 6, 2013
Published: June 24, 2013

   dx.doi.org/10.1021/nl401498t | *Nano Lett.* 2013, 13, 3287−3292

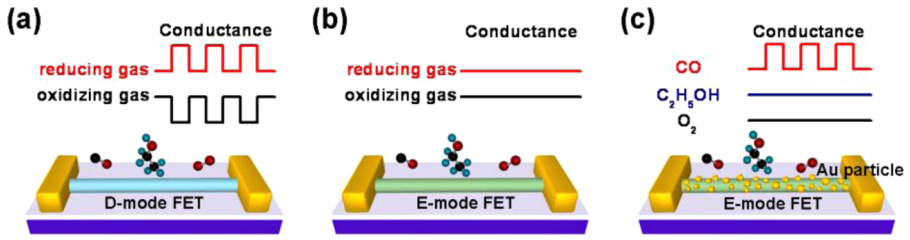

Figure 1. Illustration of the design concept "one lock to one key" sensor configuration. (a) Conventional D-mode FETs for the detection of both reducing and oxidizing gases. (b) Deep E-mode FETs with very large positive threshold voltage yield no response to any target gas. (c) Combing the deep E-mode FETs as a sensing platform, metal nanoparticles are decorated onto the nanowire channel surface to introduce the gas specific selectivity and sensitivity to the particular target gas to achieve the ideal "one lock to one key" configuration, exhibiting the unique single target gas specific response.

challenge to design and achieve the selective, real-time chemical gas sensing of specific target gas in a highly complex background with a quick response, great sensitivity, and long-lasting stability.

The present Letter provides a facile and rational design of an ideal hybrid chemical gas sensor which is constructed based on the "one key to one lock" configuration, with different sensing elements ("key") specific to various target gases ("lock") integrated into a single platform. In this work, enhancement-mode (E-mode) Mg-doped In_2O_3 nanowire FET arrays with appropriate threshold voltages are employed as the fast-response and reliable gas sensing platform, while various discrete metal nanoparticles (Au, Ag, and Pt) are decorated onto the nanowire channel to provide the gas specific selectivity for reducing gases (e.g., CO, C_2H_5OH, and H_2). The versatility of these hybrid sensors can be demonstrated with the sensitivity down to sub-ppm level with a fast response time of ~4 s, therefore enabling the direct discrimination of different target gases with unprecedented selectivity and sensitivity for the next-generation practical gas sensing.

The design concept is simple and the corresponding theoretical support can be found in Supporting Information, Figure S1. In brief, it is well-known that the electron transfer between metal oxide nanowires and gas molecules would lead to the FET conductance modulation such that oxidizing (reducing) gases can serve as electron withdrawing (donating) groups and thus change the channel carrier concentration.[22,25,26] Specifically, in the case of n-type nanowires, when an oxidizing gas (e.g., O_2) is introduced to the sensor, the following reaction happens:

$$O_2 + e^- \rightarrow 2O^-$$

This way, O_2 serves as charge accepting molecules and withdraw electrons from the surface of metal oxides, results in a reduction of the carrier concentration and consequently lowers the conductance of the nanowire channel. On the other hand, if the sensor is exposed to a reducing gas (e.g., CO), the following reaction will take place:

$$CO + O^- \rightarrow CO_2 + e^-$$

Here, the reducing gas would react with the adsorbed oxygen ions on the surface of nanowire and thus leads to an increasing carrier concentration and enhance the channel conductance. As a result, the FET conductance can be modified with the presence of different target gases (oxidizing vs reducing) in the environment as the sensor signal outputs.

Considering the requirement on low power, easy integration, and simple operation, in the current studies, the sensitivity of nanowire FET sensors is defined as the change of output current at the zero gate bias which is similar to the resistance sensors. Based on this definition, n-type depletion-mode FET would exhibit response to both reducing and oxidizing gases, since the output current, I_{ds}, increases (decreases) with the introduction of reducing gas (oxidizing gas) at V_{gs} = 0 V (Figure 1a and Supporting Information, Figure S1a). Notably, this mixed signal can only discriminate different types of gases by the pattern recognition, which is not gas-specific. In contrast, n-type E-mode FET can only give response to reducing gases but no detection for oxidizing gases. It is due to the fact that the oxidizing gas exposure would decrease the carrier concentration, shift the threshold voltage to a more positive direction, and yield a nil output current at the zero gate bias. Furthermore, for the deep E-mode FET which has a larger positive threshold voltage, even reducing gases at decent concentration can hardly switch on the transistor so that no gas can be detected (Figure 1b and Supporting Information, Figure S1b). Without the sensitivity, this deep E-mode nanowire FET configuration here can actually provide an ideal gas sensing platform due to the large nanowire surface area collecting target gas molecules, efficient electron transport transmitting output signals, as well as high crystallinity achieving long-term chemical and thermal stability. Then the gas selectivity and sensitivity can be introduced into the nanowire surface by decorating various metal nanoparticles.[27−29] More importantly, each type of these metal nanoparticles can respond to a specific gas molecule through different catalytic reaction such that this detection can achieve the almost perfect gas selectivity with high performance. For instance, it is reported that Au nanoparticles could give the excellent response to the CO oxidation activity even at subambient temperatures due to the low activation energy barrier for the CO oxidation.[30−33] In addition, Pt nanoparticles are used in the selective detection of H_2 since they can catalytically activate the dissociation of hydrogen molecules to form atomic hydrogen. The atomic hydrogen can then further diffuse to the surface of metal oxide, which facilitates the reaction between hydrogen and the adsorbed oxygen.[34−36] Also, Ag nanoparticles are illustrated to yield the outstanding sensitivity to C_2H_5OH in previous reports.[37−39] In this case, combining deep E-mode nanowire FETs with the metal nanoparticle decoration, finally, a rational-designed "one key to one lock" hybrid sensor is achieved which allows the real-time detection of a single compound among a mixture of ambient gases (Figure 1c and Supporting Information, Figure S1c).

In this design, three criteria are necessary: (i) quasi-one-dimensional metal oxide nanostructures as the sensing platform

dx.doi.org/10.1021/nl401498t | *Nano Lett.* 2013, 13, 3287−3292

which exhibits good electron mobility and chemical and thermal stability; (ii) deep E-mode FETs with appropriate threshold voltages to suppress the nonspecific sensitivity to all gases (decouple the selectivity and sensitivity away from metal oxide nanostructures); (iii) metal nanoparticle decoration onto the nanostructure surface to introduce the gas specific selectivity and sensitivity to the sensing platform. To achieve all of these requirements, Mg-doped In_2O_3 NW FET arrays are employed as sensing platform due to their controllable carrier concentration and superior electron mobility among metal oxide nanostructures.[40] Their channel surfaces are then decorated/functionalized with metal (Au, Ag, and Pt) nanoparticles by the thermal or electron beam deposition and subsequent heat treatment processes at 200 °C. Here, metal (Au, Ag, and Pt) nanoparticles are utilized to trigger the gas specific detection through the particular oxidation activity of CO, C_2H_5OH, and H_2, respectively, in a complex ambient background.

Figure 2 shows transmission electron microscope (TEM) images of In_2O_3 NWs decorated with Au, Ag, and Pt nanoparticles. It is clearly observed that the metal particles, which appear as dark spots, are distributed uniformly and densely on the surface of In_2O_3 NWs. The corresponding high-resolution transmission electron microscope (HRTEM) image (Figure 2a inset) depicts that Au particles are 2−5 nm in diameter which is similar with the other two metals (Ag and Pt). The advantages of this small size and high density distribution can effectively introduce and enhance the response toward the target gases.[16,41] High-angle annular dark-field (HAADF) image of the single In_2O_3 NW decorated with Ag particles are presented in the Figure 2b inset. Because of the strong atomic number contrast of HAADF, Ag particles appear to be bright spots in the image,[16] which again confirms the uniform particle distribution and high density here.

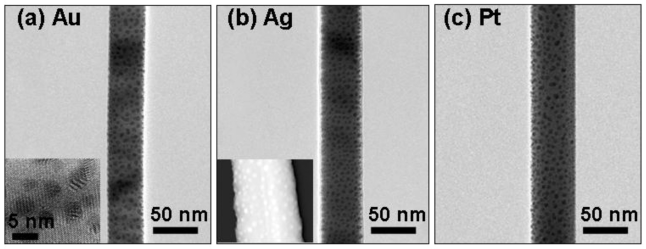

Figure 2. (a) TEM image of an Au-decorated In_2O_3 NW. The Au particles, 2−5 nm in diameter, cover the surface of the NW uniformly. (Inset) The corresponding HRTEM image of the NW. (b) TEM image of an Ag-decorated In_2O_3 NW. (Inset) The corresponding HAADF image. (c) TEM image of a Pt-decorated In_2O_3 NW.

Figure 3a illustrates the schematic of this hybrid chemical gas sensor which is used for the performance analysis in this experiment. The sensor array is composed of three individual Mg-doped In_2O_3 NW back-gate FETs. In the previous study, E-mode back-gated FETs fabricated with Mg-doped In_2O_3 NWs have been reported in detail.[40] The threshold voltage can be effectively modulated through varying Mg content in the NWs. With the metal nanoparticle decoration (Au, Ag, and Pt), this hybrid nanostructured sensor array is designed to achieve the gas specific detection of single reducing gas in a mixture of ambient gases. Figure 3b (top left) shows the optical image of the finished chemical sensor chip, where Mg-doped In_2O_3 NWs are dispersed in the center. Metal nanoparticles (Au, Ag, and Pt) are then deposited on the surface of three individual NWs, respectively, through the JEOL 6510 SEM with NPGS electron beam lithography (Supporting Information, Figure S2). The corresponding SEM image of NW FET array is shown in Figure 3b (right) while Figure 3b (bottom left) gives the high magnification SEM image of Au nanoparticles decorated Mg-doped In_2O_3 NW. Moreover, the evolution of $I_{ds}-V_{gs}$ curves with the noble metal deposition is presented in Figure 3c. The threshold voltage of pristine Mg-doped In_2O_3 NW FETs is about +10 V. With the metal deposition, it is obvious that there is significant reduction in conductance and a positive shift in threshold voltage. This phenomenon is probably due to the reduction in carrier concentration which can be explained by the "spillover effect".[42,43] According to this mechanism, metal particles catalytically activate the dissociation of molecular oxygen, whose atomic products then diffuse to surface of the metal oxide. This way, the atomic oxygen can withdraw electrons from the metal oxide and reduce the corresponding carrier concentration.[16,44]

To shed light to investigate the sensor performance, further measurements on the sensor arrays are performed: (i) at room temperature, (ii) using fresh ambient air as the background gas to simulate the practical environment and (iii) one of the four target gases (pure O_2, H_2, C_2H_5OH and CO) is added to the continuously flowing air stream at a low concentration of 100 ppm. The sensors are then measured at a fixed condition including temperature, humidity and V_{gs} sweep rate in order to avoid the disturbance of any uncertain random circumstance. In specific, the hysteresis of $I_{ds}-V_{gs}$ curve is observed when V_{gs} is

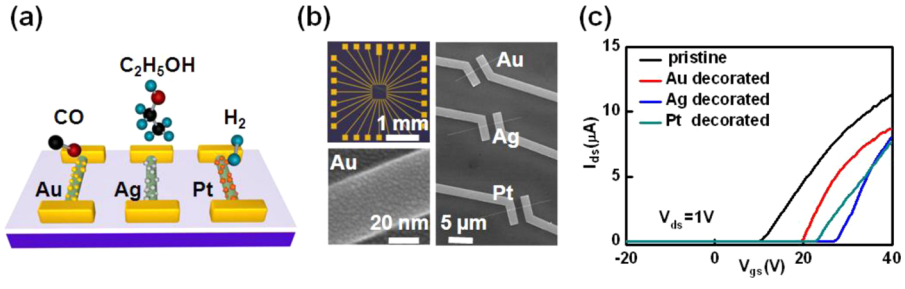

Figure 3. (a) Schematic of the hybrid chemical sensor arrays, composed of three individual Mg-doped In_2O_3 NW FETs. The surface of NWs is decorated with Au, Ag, and Pt nanoparticles, respectively. This sensor is designed to achieve the gas specific detection of single compound (CO, C_2H_5OH, and H_2) in a mixture of ambient gases. (b) Optical (top left) and SEM (right) image of the chemical sensor arrays. (bottom left) High magnification SEM image of Au decorated Mg-doped In_2O_3 NW. (c) $I_{ds}-V_{gs}$ curves at V_{ds} = 1 V for the back-gated Mg-doped In_2O_3 FETs with and without the metal decoration.

dx.doi.org/10.1021/nl401498t | Nano Lett. 2013, 13, 3287−3292

swept from −40 V to +40 V and back to −40 V; however, the hysteresis does not show any significant difference upon the exposure to different gases (Supporting Information, Figure S3). Additionally, there is no obvious hysteresis for I_{ds}-V_{ds} curves as V_{ds} is swept from 0 V to +1 V and back to 0 V (Supporting Information, Figure S4). All of these suggest the consistency of our hybrid sensor performance operated at room temperature. The representative I_{ds}−V_{gs} curves of Au decorated E-mode FETs is then shown in Figure 4a. Obviously, at V_{gs} = 0 V, only diluted CO brings about a remarkable change in the output current due to the significantly enhanced catalytic activity for CO oxidation induced by the Au nanoparticles. Although other reducing gases (H_2 and C_2H_5OH) would also shift the threshold voltage to the negative direction slightly as well, the alteration is not sufficient to switch the FETs to on-state. In addition, the oxidizing gas (O_2) causes the threshold voltage a positive shift which infers that the FETs is still in off-state at V_{gs} = 0 V. This way, the sensor can indeed provide the almost perfect gas selectivity to CO in this hybrid configuration. Figure 4 panels b, c, and d represent the I_{ds}−V_{ds} characteristics at V_{gs} = 0 V for Au-decorated, Ag-decorated, and Pt-decorated FETs. At low V_{ds}, I_{ds} increases linearly with V_{ds}, indicating that ohmic contacts are successfully formed between the NWs and the source/drain electrodes, regardless of the metal-functionalization. Importantly, the gas specific enhancement in the FET conductance can be clearly demonstrated with Au, Ag, and Pt nanoparticles decorated nanowire channels for the selective detection of CO, C_2H_5OH, and H_2, respectively. Notably, an absence of conductance change for the O_2 exposure also can be observed, which further confirms the gas selectivity of the sensor configuration in this work.

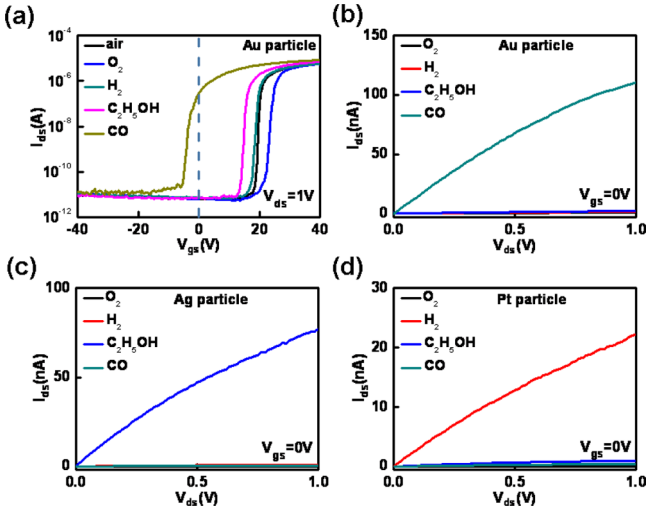

Figure 4. (a) I_{ds}−V_{gs} curves at V_{ds} = 1 V for the Au decorated E-mode FETs upon the exposure to various gases at a low concentration of 100 ppm. A family of I_{ds}−V_{ds} curves at V_{gs} = 0 V for (b) Au decorated, (c) Ag decorated, and (d) Pt decorated E-mode FETs toward the gas specific detection of O_2, H_2, C_2H_5OH, and CO.

Besides the selectivity, sensitivity is another important requirement for the high-performance chemical gas sensors, and the experimental findings on the sensor sensitivity will be discussed in this section. The sensor sensitivity (S) is defined as $S = I_g/I_a$, in which I_g and I_a are, respectively, the steady-state output current values measured with the analytic gas added to the air stream and just the air stream alone. Figure 5a plots the current change for Au decorated E-mode FET sensor arrays at V_{ds} = 1 V and V_{gs} = 0 V as a function of time. Six cycles are successively recorded, corresponding to six different CO/air concentrations ranging from 100 ppm down to 0.5 ppm, respectively. As predicted, the introduction of these decreasing CO concentrations would lead to a little reduction of the nanowire carrier concentration which subsequently increases the channel resistivity and thus lowers the output current. Obviously, the sensor exhibits a nearly linear response to CO in the range of 0.5−100 ppm (Figure 5b). Such favorable characteristics indicate that the present sensor is very suitable for the detection of CO at low levels. The largest response, up to 3 orders of magnitude (~2200), is observed upon the 100 ppm CO exposure. This is one of the best values so far reporting for the metal oxide nanomaterials based CO gas sensors, which can be ascribed to the high on/off output current ratio of these deep E-mode FETs employed here.

Moreover, high-performance sensors are also expected to respond efficiently (e.g., in a short response time) for the target gases for practical applications. Here, the response time is

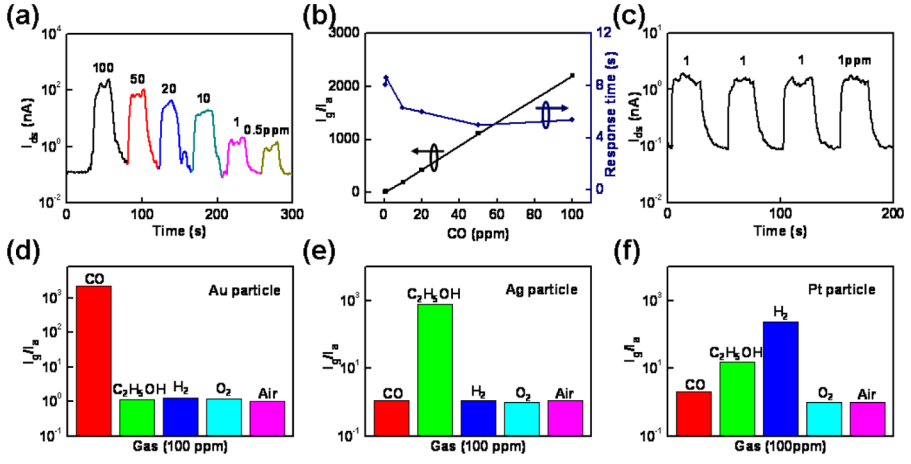

Figure 5. (a) Current change of the Au-decorated sensor upon exposure to 0.5, 1, 10, 20, 50, and 100 ppm CO gas at V_{ds} = 1 V and V_{gs} = 0 V. (b) The variation of sensitivity and response time of the E-mode FET sensor arrays with the different concentrations of CO. (c) Performance reproducibility of Au decorated E-mode FET sensor arrays to the 1 ppm CO exposure. Bar chats summarize the sensitivity of the (d) Au-decorated, (e) Ag-decorated, and (f) Pt-decorated E-mode FET sensor arrays to the different gas at 100 ppm concentration.

dx.doi.org/10.1021/nl401498t | Nano Lett. 2013, 13, 3287−3292

defined as the time required reaching 90% of the total response of the output current upon exposure to the target gas. Figure 5b as well illustrates the typical response time of the Au decorated E-mode FET sensor arrays to different CO concentrations. The response time to the range of 0.5−100 ppm in the CO concentration is around 8 to 4 s, accordingly. These times are short enough for practical applications. To further check for the performance stability, $I_{ds}-V_{gs}$ curves at V_{ds} = 1 V upon 100 ppm CO exposure are measured several times at intervals of 20 min (Supporting Information, Figure S5). There is no significant change in both hysteresis and threshold voltage, indicating the good stability of the sensor in the test environment. In addition, the response to 1 ppm CO exposure is measured for several cycles, as shown in Figure 5c. Nearly constant sensitivity to this 1 ppm CO introduction shows that the sensor has good reproducibility. The bar chats of Figure 5d−f summarize the response of the sensor arrays to different target gases (at 100 ppm concentration). Apparently, sensors decorated with Au and Ag nanoparticles exhibit excellent performance in both selectivity and sensitivity to CO and C_2H_5OH, respectively. Although Pt decorated sensors show a slight fall in the selectivity, their performance can be further improved through modulating the threshold voltage to more positive values, therefore providing the better discrimination of H_2 among the other gases.

In summary, the presented work rationally designs an ideal "one key to one lock" hybrid sensor configuration which can be used in the selective detection of a specific reducing gas among the complex ambient background. In comparison with the conventional chemical sensors whose selectivity is based on reading out overlapping signals of several different target gases, this rational-designed sensor has a unique advantage in the specific efficient response to one particular target gas. To demonstrate our rational design for the highly selective reducing gas sensor, Mg-doped In_2O_3 NW E-mode FET arrays are decorated with metal nanoparticles (Au, Ag, and Pt) and employed as the illustrative prototypes. The sensors are operated and tested at room temperature for their ability to distinguish among three reducing gases (CO, H_2, and C_2H_5OH), which they are able to differentiate unequivocally. Furthermore, the sensors also exhibit high sensitivity, low power, and fast response, which are important for the practical applications. As a result, this unique approach can indeed facilitate a new avenue to nanowire-based highly selective and sensitive gas sensors to impact broadly from chemical sensors to biosensors.

■ ASSOCIATED CONTENT

Supporting Information

Ideal $I_{ds}-V_{gs}$ curves which are used to support the design concept (Figure S1); illustration of the fabricating process of metal decorated E-mode nanowire FET sensor arrays (Figure S2); hysteresis of $I_{ds}-V_{gs}$ curves for the Au decorated E-mode FET (Figure S3); hysteresis of $I_{ds}-V_{gs}$ curves for the Au decorated E-mode FET (Figure S4); $I_{ds}-V_{gs}$ curves at V_{ds} = 1 V upon 100 ppm CO exposure to check for the performance stability (Figure S5). This material is available free of charge via the Internet at http://pubs.acs.org.

■ AUTHOR INFORMATION

Corresponding Author

*E-mail: liaolei@whu.edu.cn (L.L.); johnnyho@cityu.edu.hk (J.C.H.).

Notes

The authors declare no competing financial interest.

■ ACKNOWLEDGMENTS

We acknowledge the 973 grant of MOST (no. 2011CB932704), MOE (NCET-10-0643 and 20120141110054), and NSFC grants (nos. 11104207, 61222402, 91123009, and 612501100540), Hubei Province Natural Science Foundation (2011CDB271), the Grant of State Key Laboratory of Silicate Materials for Architectures in Wuhan University of Technology (no. SYSJJ2013-05), and the General Research Fund of the Research Grants Council of Hong Kong SAR, China, under Project Nos. CityU 101210 and CityU 101111.

■ REFERENCES

(1) Kong, J.; Franklin, N. R.; Zhou, C. W.; Chapline, M. G.; Peng, S.; Cho, K. J.; Dai, H. J. *Science* **2000**, *287*, 622−625.
(2) Kolmakov, A.; Moskovits, M. *Annu. Rev. Mater. Res.* **2004**, *34*, 151−180.
(3) Zhang, D. H.; Liu, Z. Q.; Li, C.; Tang, T.; Liu, X. L.; Han, S.; Lei, B.; Zhou, C. W. *Nano Lett.* **2004**, *4*, 1919−1924.
(4) Pengfei, Q. F.; Vermesh, O.; Grecu, M.; Javey, A.; Wang, O.; Dai, H. J.; Peng, S.; Cho, K. J. *Nano Lett.* **2003**, *3*, 347−351.
(5) Li, J.; Lu, Y. J.; Ye, Q.; Cinke, M.; Han, J.; Meyyappan, M. *Nano Lett.* **2003**, *3*, 929−933.
(6) Murray, B. J.; Walter, E. C.; Penner, R. M. *Nano Lett.* **2004**, *4*, 665−670.
(7) Gao, X. P. A.; Zheng, G. F.; Lieber, C. M. *Nano Lett.* **2010**, *10*, 547−552.
(8) Cheng, Y.; Xiong, P.; Yun, C. S.; Strouse, G. F.; Zheng, J. P.; Yang, R. S.; Wang, Z. L. *Nano Lett.* **2008**, *8*, 4179−4184.
(9) Joshi, R. K.; Hu, Q.; Am, F.; Joshi, N.; Kumar, A. *J. Phys. Chem. C* **2009**, *113*, 16199−16202.
(10) Kolmakov, A.; Zhang, Y. X.; Cheng, G. S.; Moskovits, M. *Adv. Mater.* **2003**, *15*, 997.
(11) Cui, Y.; Wei, Q. Q.; Park, H. K.; Lieber, C. M. *Science* **2001**, *293*, 1289−1292.
(12) Liu, H. Q.; Kameoka, J.; Czaplewski, D. A.; Craighead, H. G. *Nano Lett.* **2004**, *4*, 671−675.
(13) Zeng, Z.; Wang, K.; Zhang, Z.; Chen, J.; Zhou, W. *Nanotechnology* **2009**, *20*, 045503.
(14) Shen, G.; Chen, P.-C.; Ryu, K.; Zhou, C. *J. Mater. Chem.* **2009**, *19*, 828−839.
(15) Li, C.; Zhang, D. H.; Liu, X. L.; Han, S.; Tang, T.; Han, J.; Zhou, C. W. *Appl. Phys. Lett.* **2003**, *82*, 1613−1615.
(16) Kolmakov, A.; Klenov, D. O.; Lilach, Y.; Stemmer, S.; Moskovits, M. *Nano Lett.* **2005**, *5*, 667−673.
(17) Baik, J. M.; Zielke, M.; Kim, M. H.; Turner, K. L.; Wodtke, A. M.; Moskovits, M. *ACS Nano* **2010**, *4*, 3117−3122.
(18) Comini, E.; Faglia, G.; Sberveglieri, G.; Pan, Z. W.; Wang, Z. L. *Appl. Phys. Lett.* **2002**, *81*, 1869−1871.
(19) Choi, J.-K.; Hwang, I.-S.; Kim, S.-J.; Park, J.-S.; Park, S.-S.; Jeong, U.; Kang, Y. C.; Lee, J.-H. *Sens. Actuators B* **2010**, *150*, 191−199.
(20) Sysoev, V. V.; Button, B. K.; Wepsiec, K.; Dmitriev, S.; Kolmakov, A. *Nano Lett.* **2006**, *6*, 1584−1588.
(21) Yao, K.; Caruntu, D.; Wozny, S.; Huang, R.; Ikuhara, Y. H.; Cao, B.; O'Connor, C. J.; Zhou, W. *J. Mater. Chem.* **2012**, *22*, 7308−7313.
(22) Chen, P.-C.; Ishikawa, F. N.; Chang, H.-K.; Ryu, K.; Zhou, C. *Nanotechnology* **2009**, *20*, 125503.
(23) Chen, P.-C.; Shen, G.; Zhou, C. *IEEE T. Nanotechnol.* **2008**, *7*, 668−682.
(24) McAlpine, M. C.; Ahmad, H.; Wang, D.; Heath, J. R. *Nat. Mater.* **2007**, *6*, 379−384.
(25) Yao, K.; Caruntu, D.; Zeng, Z.; Chen, J.; O'Connor, C. J.; Zhou, W. *J. Phys. Chem. C* **2009**, *113*, 14812−14817.

(26) Liao, L.; Lu, H. B.; Li, J. C.; He, H.; Wang, D. F.; Fu, D. J.; Liu, C.; Zhang, W. F. *J. Phys. Chem. C* **2007**, *111*, 1900−1903.
(27) Wang, H. T.; Kang, B. S.; Ren, F.; Tien, L. C.; Sadik, P. W.; Norton, D. P.; Pearton, S. J.; Lin, J. *Appl. Phys. Lett.* **2005**, *86*, 243503.
(28) Chen, X. H.; Moskovits, M. *Nano Lett.* **2007**, *7*, 807−812.
(29) Baik, J. M.; Kim, M. H.; Larson, C.; Yavuz, C. T.; Stucky, G. D.; Wodtke, A. M.; Moskovits, M. *Nano Lett.* **2009**, *9*, 3980−3984.
(30) Kandoi, S.; Gokhale, A. A.; Grabow, L. C.; Dumesic, J. A.; Mavrikakis, M. *Catal. Lett.* **2004**, *93*, 93−100.
(31) Haruta, M. *Gold Bull.* **2004**, *37*, 27−36.
(32) Schubert, M. M.; Hackenberg, S.; van Veen, A. C.; Muhler, M.; Plzak, V.; Behm, R. J. *J. Catal.* **2001**, *197*, 113−122.
(33) Choudhary, T. V.; Goodman, D. W. *Catal. Today* **2002**, *77*, 65−78.
(34) Shen, Y.; Yamazaki, T.; Liu, Z.; Meng, D.; Kikuta, T. *J. Alloys Compd.* **2009**, *488*, L21−L25.
(35) Tien, L. C.; Sadik, P. W.; Norton, D. P.; Voss, L. F.; Pearton, S. J.; Wang, H. T.; Kang, B. S.; Ren, F.; Jun, J.; Lin, J. *Appl. Phys. Lett.* **2005**, *87*, 222106.
(36) Kryliouk, O.; Park, H. J.; Wang, H. T.; Kang, B. S.; Anderson, T. J.; Ren, F.; Pearton, S. J. *J. Vac. Sci. Technol., B* **2005**, *23*, 1891−1894.
(37) Joshi, R. K.; Kruis, F. E. *Appl. Phys. Lett.* **2006**, *89*, 153116.
(38) Hu, P.; Du, G.; Zhou, W.; Cui, J.; Lin, J.; Liu, H.; Liu, D.; Wang, J.; Chen, S. *ACS Appl. Mater. Interfaces* **2010**, *2*, 3263−3269.
(39) Zhang, Y.; Zheng, Z.; Yang, F. *Ind. Eng. Chem. Res.* **2010**, *49*, 3539−3543.
(40) Zou, X.; Liu, X.; Wang, C.; Jiang, Y.; Wang, Y.; Xiao, X.; Ho, J. C.; Li, J.; Jiang, C.; Xiong, Q.; Liao, L. *ACS Nano* **2013**, *7*, 804−810.
(41) Franke, M. E.; Koplin, T. J.; Simon, U. *Small* **2006**, *2*, 36−50.
(42) Khoobiar, S. *J. Phys. Chem.* **1964**, *68*, 411−412.
(43) Boudart, M.; Vannice, M. A.; Benson, J. E. *Z. Phys. Chem. (Frankfurt)* **1969**, *64*, 171−177.
(44) Kim, S. S.; Park, J. Y.; Choi, S.-W.; Kim, H. S.; Na, H. G.; Yang, J. C.; Kim, H. W. *Nanotechnology* **2010**, *21*, 415502.